JETSAN 2021

Device Attitude and Real-Time 3D Visualization: An Interface for Elderly Care ☆

M. Abbas [a,*], M. Saleh [a], J. Prud'Homm [a], F. Lemoine [a], D. Somme [b], R. Le Bouquin Jeannès [a]
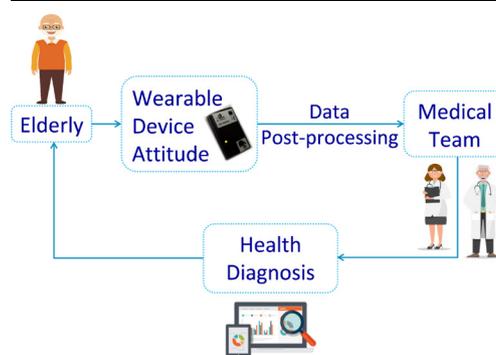
[a] Univ Rennes, Inserm, LTSI UMR 1099, F-35000 Rennes, France
[b] CHU de Rennes, Service de Gériatrie, F-35000 Rennes, France

HIGHLIGHTS

- 3D visualization of wearable device attitude.
- A reliable tool for activity monitoring.
- The importance of sensing unit (IMU vs MARG).
- Comparison between orientation filters.

GRAPHICAL ABSTRACT

ARTICLE INFO

ABSTRACT

Objective: this paper presents an innovative graphical user interface to visualize the attitude of a sensing device in a three-dimensional space, serving a wide-range of medical applications.
Material and methods: based on inertial measurement units (IMU) or on magnetic, angular rate and gravity (MARG) sensors, a processing unit provides Euler angles using a sensor fusion technique to display the orientation of the device relative to the Earth frame in real-time. The device is schematized by linking six polygonal regions, and is subject to sequential rotations by updating the graph each 350 ms. We conduct comparative studies between the two sensing devices, *i.e.* IMUs and MARGs, as well as two orientation filters, namely Madgwick's algorithm and Mahony's algorithm.
Results: the accuracy of the system is reported as a function of (i) the sampling frequency, (ii) the sensing unit, and (iii) the orientation filter, following two elderly care applications, namely fall risk assessment and body posture monitoring. The experiments are conducted using public datasets. The corresponding results show that Madgwick's algorithm is best suited for low sampling rates, whereas MARG sensors are best suited for the detection of postural transitions.
Conclusion: this paper addresses the different aspects and discusses the limitations of attitude estimation systems, which are important tools to help clinicians in their diagnosis.

1. Introduction

In the past decades, minimized electronic sensors have been known for their low price, and their widespread use in the health-care domain [8]. The integration of these sensors in wearable devices or smartphones has been shown to be reliable for many monitoring systems and healthcare applications [13]. In the literature, Hwang et al. have proposed a hierarchical deep learning model to recognize human activities [10]. They adopted a fusion technique using some physiological sensors such as photoplethysmography and electrodermal activity as well as inertial sensors like an accelerometer. Sevil et al. [20] have inspected wristband data including acceleration and other physiological measurements to detect physical activity and characterize physiological stress. Tri-axial accelerometry using smartphones was also investigated to monitor obstructive sleep apnea at home [7]. Han et al. [9] developed a wearable sensing solution for forward head posture monitoring. The system is based on a tri-axial magnetometer paired with a miniature permanent magnet, and fused with an accelerometer. Now, sensor fusion techniques have been developed to estimate the attitude of sensing devices [17]. In other words, the orientation of the device relative to the Earth frame is measured by merging data acquired from a tri-axial accelerometer and a tri-axial gyroscope, or from these two sensors and a tri-axial magnetometer, thus forming an attitude and heading reference system (AHRS). These approaches are useful for human motion tracking [21], which is the base of several medical solutions. Two types of accelerometers exist. The first one concerns capacitive accelerometers, also known as micro-electro-mechanical systems (MEMS). These accelerometers depend on a change in electrical capacitance to measure acceleration. The second type refers to piezoelectric accelerometer, which is made of a quartz crystal. A force acting on the piezoelectric element is produced when the accelerometer is moving. A charge output, generated from these vibrations, is proportional to the applied force and is used to measure acceleration. The first type has the advantage of measuring the static acceleration caused by the gravity. This measurement is important for orientation estimation techniques. This justifies why MEMS sensors are preferred for this task.

Given these aforementioned elements, we proposed in a previous work [2] a graphical user interface (GUI) to visualize the attitude of a sensing unit in real-time (called D-SORM). Once fed by acquired data, particularly acceleration, angular velocity, and magnetic fields, the processing units estimate the orientation of the device relative to Earth frame. This orientation can be visualized by plotting the sensor in a 3-dimensional coordinate system, and by rotating the vertices and the faces of the plot to update the graph periodically. The present paper extends the previous work in different aspects, particularly in terms of input signals, orientation filters (*i.e.* sensor-fusion technique), and sampling frequency. A new module is added, where the subject can select the type of sensing unit (acquired data) together with the orientation filter. Firstly, the orientation can now be estimated before and after adding a magnetometer to the input source, thus inspecting the value of magnetic fields in this context. Secondly, the performances of two widely used orientation filters are evaluated and compared. Examining the way of estimating the device attitude is important to increase the reliability of the system and decrease the required computational load if possible. Thirdly, the effect of the sampling frequency on the accuracy is also studied in this paper. Finally, some drawbacks and limitations related to orientation estimation systems, as well as some practical considerations are discussed. Analyzing medical reports and questioning patients are not always sufficient to accurately check their health. Clinicians may need to visualize the orientation of wearable devices to assess the movements of their patients (or a certain event like a fall) and/or to
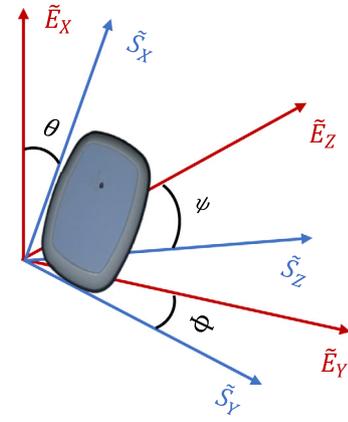

Fig. 1. A sensing device, with its corresponding frame ($\tilde{S}$) and the Earth frame ($\tilde{E}$). (For interpretation of the colors in the figure(s), the reader is referred to the web version of this article.)

restore them to normal behavior. The proposed tool answers these questions.

The remainder of the paper is organized as follows. Section 2 discusses the principle of orientation estimation algorithms and describes the functionalities and the characteristics of the interface. Some real world examples are given in section 3 allowing comparative studies, including the type of the sensing unit, the input data, as well as the orientation filter and the effect of the sampling frequency on the accuracy of the system. Finally, section 4 addresses some limitations and practical considerations, whereas section 5 concludes the paper.

2. Real-time orientation display via GUI

2.1. Principle of attitude estimation

The orientation estimation of a device with respect to an inertial frame or reference is done using sensor fusion techniques. Reading multimodal data from different sources gives valuable information to understand and symbolize the motion of the sensing device. Inertial measurement units (IMUs), which consist of an accelerometer and a gyroscope, are able to monitor translational and rotational motions. On the other hand, magnetic, angular rate and gravity (MARG) devices include a third sensor, namely a magnetometer. This type of sensing unit has the advantage of measuring the attitude relative to the Earth magnetic field, which could be an added-value to an AHRS and thus increases its precision. The choice of the sensing device depends on the requirements of the developed system. An IMU might be sufficient for some applications. In this paper, both devices (IMU and MARG) are investigated in the next sections.

Fig. 1 illustrates a sensing device (IMU or MARG), with its corresponding coordinate system (sensor frame) in black, and in the Earth frame $\tilde{E}$ in red. The goal is to estimate the orientation of the sensor frame $\tilde{S}$ relative to $\tilde{E}$. This orientation is represented by Euler angles [14], defined by subsequent rotations of ϕ around $\tilde{E}_X$, θ around $\tilde{E}_Y$, and ψ around $\tilde{E}_Z$. Hence, data acquired from inertial sensors are processed to estimate the sequence of Euler angles, using Kalman filters [6], gradient descent step [11], quaternion representation [5]... To our knowledge, the two widely used orientation filters are the one proposed by Mahony et al. [16] and by Madgwick et al. [15]. The effectiveness of these algorithms has been proven at relatively low computational cost. Moreover, they both have low latency with a response time less than 300 ms [2]. This fast response ensures a higher frame rate and therefore a smoother 3D visualization (detailed in section 2.2). It is worth noting that the output of these algorithms are three time-series,
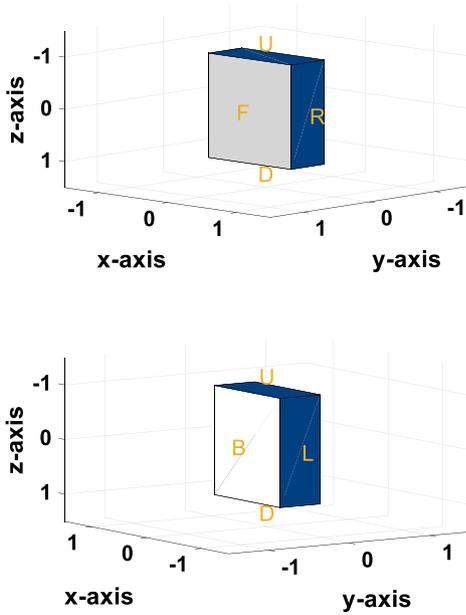
Fig. 2. Two different views of the plotted sensing device in a three-dimensional space, and its corresponding labels in yellow.

having the same sampling rate of the deployed modalities, representing the progression of Euler angles over time. The performance of both algorithms is considered in the next sections of this paper.

2.2. Visualization in a 3D space

A graphical user interface (GUI) tool was developed on Matlab to display the orientation of a sensing device based on its acquired data. The sensing device in Fig. 1 is symbolized by plotting three pairs of polygonal regions using the patch function by initializing the coordinates of each vertex. The vertices are connected in a specified order so that each of these six regions represents one face of this device. Afterwards, each region is colored using hexadecimal codes for RGB. For instance, the color of the frontal zone is set to grey (c_1), and that of the backward zone to white (c_2), while the remaining faces are colored in dark blue (c_3). Moreover, the six regions are labeled using the following letters: **'U'** which stands for up, **'D'** for down, **'L'** for left, **'R'** for right, **'F'** for front, and **'B'** for back. The color of these letters is set to yellow. Fig. 2 illustrates the plotted device in a three-dimensional space. This is the initial position of the device, *i.e.* at the beginning of the algorithm ($t = 0$).

Now, the Euler angles are updated after the acquisition of each data-point from the inertial sensors. The orientation filter reads data from sensors, processes them, and fuses them to estimate the angles. Each 350 ms, the graph is updated by rotating the simulated device and the corresponding labels, according to the output of the filter. This frame rate, *i.e.* the frequency at which consecutive images appear on a display, seems adequate for the human eye. This update is done by pivoting the centroids of the device faces (localized using the coordinates of any two opposite vertices) around the axes, using the estimated Euler angles [2]: θ around the x-axis, ϕ around the y-axis, and ψ around the z-axis.

Two modes can be considered. The real-time mode, where data are sent continuously to a remote server using a Bluetooth dongle (if the wearable sensor includes a Bluetooth module) or via internet (wifi) for example. The second one is the replay mode, where data have been acquired beforehand. Two modules are added to this tool. Explicitly, the type of the sensing device (IMU or MARG) and the orientation filter (Mahony et al. [16] or Madgwick et al. [15]) are chosen before launching the algorithm. When a MARG

sensor is chosen, the magnetic distortion compensation unit is activated automatically to process magnetic fields. This manipulation increases the flexibility of the proposed system.

3. The aspects of orientation estimation systems via real world applications

The proposed tool, *i.e.* orientation estimation and visualization of the sensing device, serves a wide-range of healthcare applications. In a previous work [2], a machine-learning based human activity recognition architecture was developed to inspect the orientation of the wearable sensor and predict the performed activity. The output classes were transient activities like sitting-down/standing and lying-down/rising-up, cyclic activities like walking and climbing/descending stairs, staying still (inactivity) and falling. In this section, two medical applications are considered, namely fall assessment and body posture monitoring. The first one characterizes the fall incident when it occurs. The second one detects the body posture when the subject is inactive (staying still), particularly sitting, standing, and lying. We also conduct comparative studies involving Mahony's filter *vs* Madgwick's filter, the effect of the sampling frequency F_s on the accuracy, and IMU *vs* MARG.

3.1. Fall risk assessment

Falls are one of the main causes of mortality in elderly. While most of the proposed solutions target fall detection, the clinician may need to evaluate this fall by observing the successive movements of the wearable device during this fall. The initial state of the human body (standing, sitting, lying, walking, etc.) which precedes the fall, the velocity of the impact, and the direction of the fall (forward, backward, lateral) are important factors from a medical point of view. The proposed tool answers all these questions and provides an added-value for the practitioner. Now, we address the real world situation, resorting to the FallAllD public dataset [19]. This dataset contains data acquired from tri-axial accelerometers, tri-axial gyroscopes, and tri-axial magnetometers, including human falls. The subjects wore a necklace device while simulating falls and ADLs. As indicated by its name (<u>Fall</u> in <u>All</u> <u>D</u>irections), this dataset consists of a wide-range of falls in different directions starting with different postures (standing, sitting, lying). In this section, the ability of detecting the direction of falls (forward, backward, lateral) is investigated using machine learning models (tri-class classification), while conducting two comparative studies, namely (i) Madgwick's algorithm *vs* Mahony's algorithm (orientation filters) and IMU *vs* MARG (sensing unit).

Madgwick's filter vs Mahony's filter - Both algorithms were tested to calculate Quaternions then Euler angles. For reasons of clarity, only necklace IMUs (accelerometer + gyroscope) are considered in this section. Falls were selected from FallAllD then segmented using seven different 6-second windows: the one centered on the peak (impact) and six others shifted by ±250 ms, ±500 ms, and ±750 ms. It is worth mentioning that the choice of 6-second windows is based on previous studies [1,2], where this length appeared to be suitable for human movements identification and tracking. This segmentation is important to reflect the behavior of the machine learning classifier in real world situations. The model should be trained over different positions seeing that the sliding window is not controlled in real-time. The previous operations resulted in 3325 samples (time-series). Each time-series representing an angle (ϕ, θ, ψ) is divided into three equal sub-segments of 2 s, and the mean value of each sub-segment is calculated, resulting in 9 features in total. Moreover, the correlation between each pair of
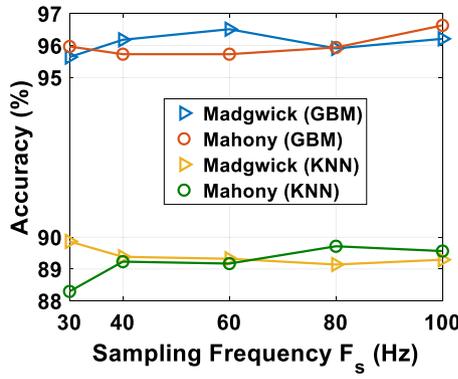
Fig. 3. The effect of the sampling frequency F_s on the accuracy of the machine learning classifier following both orientation filters (Madgwick's filter and Mahony's filter).

Fig. 4. The outcome of the tri-class classification of GBM per fall direction in terms of recall and precision using 1-*vs*-all strategy.

angles is calculated as the ratio of the covariance to the product of the standard deviations, resulting in 3 features. Explicitly, the correlation ζ between two angles α_1 and α_2 is equal to:

$$\zeta(\alpha_1, \alpha_2) = \frac{cov(\alpha_1, \alpha_2)}{\sigma_{\alpha_1} \sigma_{\alpha_2}} \qquad (1)$$

The previous operations of feature extraction result in a feature vector of length 12 (9+3 features). Hence, the final dataset is a 3325×12 matrix, where each row represents a feature vector of a certain fall, and each column represents an element of the feature vector. Each fall is labeled according to its direction, *i.e.* forward falls are labeled as C_1, backward falls as C_2, and lateral falls as C_3.

Three machine learning models were applied using repeated 10-fold cross validation (number of repeats is equal to 3), namely k-Nearest Neighbor (KNN) with $k = 5$, Random Forest (RF) with 50 estimators and a depth equal to 5, and Gradient Boosting Machine (GBM) with 100 estimators, a depth equal to 5, and a learning rate of 0.1. The acceleration and angular velocity signals were down-sampled to test the effect of the sampling frequency F_s on the accuracy of the model. GBM and RF achieved similar results, with the former being the better performer, while KNN achieved relatively lower results. For readability purposes, Fig. 3 illustrates the corresponding results for both GBM and KNN. It is obvious that the accuracy of both classifiers is somewhat saturated when Euler angles are computed using Madgwick's filter. Globally, Madgwick's algorithm outperforms slightly that of Mahony for low F_s. Meanwhile, the latter achieves moderately better results for higher F_s (> 60 Hz). Mahony's orientation filter requires higher sampling rate compared to that of Madgwick, which might increase the computational load and thus the power consumption of the system. The choice of orientation filter depends on the application, whether it requires a high sampling rate or not.

Fig. 4 illustrates the precision and recall for each class (*i.e.* fall direction) using the 1-*vs*-all strategy, based on the results of the GBM. This tri-class classification is highly sensitive to forward falls (highest recall value of 97.28%). Meanwhile, it is more precise when it comes to backward and lateral falls (precision of 96.94% and 96.51% respectively). Basically, backward falls generate the least amount of false detection.

Sensing Unit: IMU vs MARG - The focus is now on the comparison between both sensing units, *i.e.* IMU (accelerometer + gyroscope) and MARG (accelerometer + gyroscope + magnetometer). For reasons of clarity, Madgwick's algorithm is used as orientation filter with F_s being fixed to 60 Hz. This choice was based on the aforementioned results (see Fig. 3) and on Madgwick's internal report [14], where it was demonstrated that a sampling rate higher than 50 Hz ensures a high level of performance. Fig. 5 illustrates the time-series of the estimated Euler angles from both sensing units,
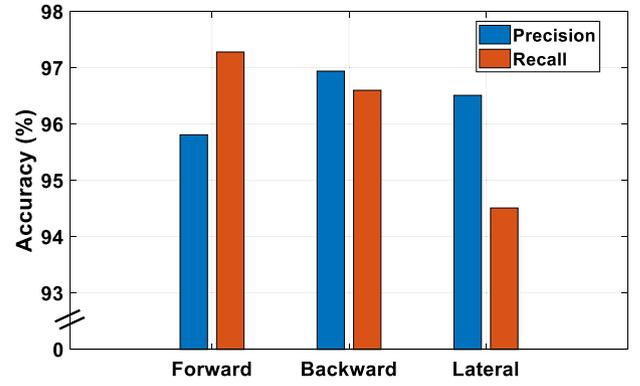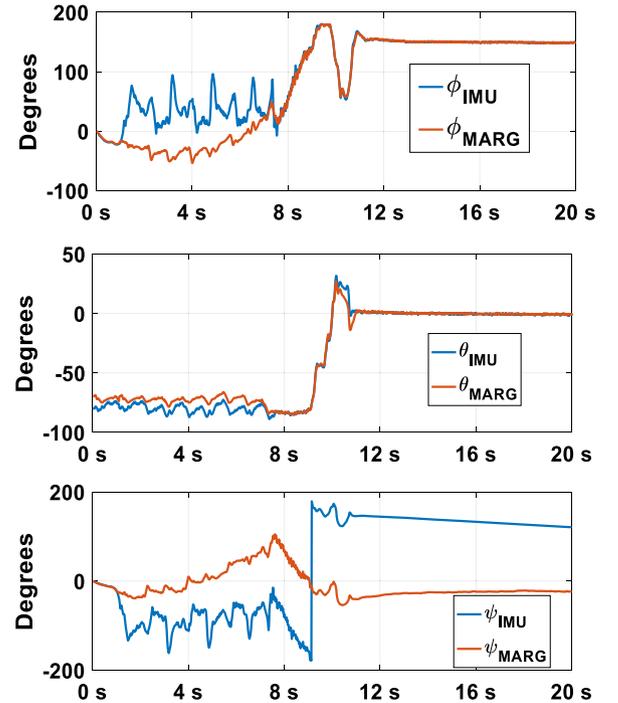

Fig. 5. The estimation of Euler angles using (i) IMU and (ii) MARG sensors using Madgwick's algorithm.

representing a fall forward from walking caused by syncope (fainting) without recovery. It is clear from this figure that the subject was walking during the first 8 seconds, where the MARG sensor shows that $\phi \approx 0°$, $\theta \approx -90°$, and $\psi \approx 0°$ (the subject was standing). This phase is called pre-impact phase. Afterwards, the impact phase was located between the 8th and 12th seconds (the shock is around the 10th second), where a change in angles occurred. The subject was lying on the floor (inactive) for the remaining 8 seconds. A video has been created to display the orientation of the device during this fall, using both estimations (see Appendix).

The variability of the IMU estimation is higher while the subject was walking, even though the three angles are not changing during this phase. When it comes to MARG, the orientation estimation is smoother. Moreover, concerning the angle ψ, a certain phenomenon appears in the IMU estimation. A sudden change from $-180°$ to $180°$ occurs between the 9th and 10th seconds (when the body was on the verge of hitting the floor), due to the effect of the angular velocity. From 3D visualization point of view (see video), there is no rotation around this axis. This means that the device kept the same inclination. Now, from a signal point of view, this

Table 1

Comparative study between both sensing units, namely IMU and MARG.

	Phase	Angle	IMU	MARG
Variability$^\sigma$	Pre-impact	All†	18.12	8.22
Filtering*	Impact	ψ	55.36	0.93
Correlation	All‡	(ψ, θ)	0.93	0.63
Variability$^\sigma$	Post-impact	All†	1.2	0.6
Slope	Post-impact	ψ	-3°/s	0.39°/s

† mean value of the results from each angle.
‡ the whole window.
* the variance of the filtered signal.
$^\sigma$ the standard deviation of the signal.

switch from $-180°$ to $180°$ means that a certain rotation occurred around the z-axis. In this case, by using filtering methods or correlation for example, a certain deviation would be detected, since the signal level changed (see blue signal in Fig. 5). Additionally, the angle ψ estimated from IMU is decreasing during the post-impact phase, even though the subject is inactive after the fall. All the aforementioned remarks may lead to biased results when it comes to the estimation of fall direction and the final body state (after the impact on the ground). Although these phenomena may not be visible in the visualization process (as displayed in the video), they have their effects on the processing units and the detection modules. To quantify these observations, we calculated the variability of the pre-impact phase (standard deviation of the signal) when the subject is moving, and that of the post-impact phase when he is inactive, the variance of the impact phase after being subject to a high-pass filter, the correlation between two pairs of angles, and the slope of the curve of angle ψ during the post-impact phase. Table 1 illustrates the corresponding results. The variability of IMU is considerably higher when the subject is moving, but is close to that of MARG during inactivity periods. Ideally, this parameter should be small when the body trunk is moving without changing its posture, and equal to 0 when the subject is inactive. The phenomenon of angle ψ is visible in the variance of the filtered signal (2nd row of Table 1) and the correlation between ψ and θ (3rd row of Table 1). A considerably high value of 55.36 indicates that high frequencies were detected in the signal. Hence, if the postural transitions detection algorithm is based on filtering methods, its reliability will be affected. Besides, while using IMU, ψ and θ are correlated (with a value of 0.93). This is not the case when the estimation is done using MARG. Indeed, the simulated fall involved a rotation around the y-axis (angle θ), whereas the z-axis kept the same orientation before and after the shock. Therefore, both angles θ and ψ should not be correlated. Finally, the slope of IMU (when it comes to ψ) is relatively higher compared to that of MARG, which is close to 0. Consequently, and based on the previous observations, MARG sensors may be preferred for postural transitions and recurrent movements (like walking), since they involve higher degrees of freedom, thus having an advantage over IMUs by providing robust orientation estimation.

3.2. Body posture monitoring

Another medical application is the distribution of the body posture over the course of a day. In other words, the idea is to detect the periods when the subject is sitting, standing, and lying. This information is valuable for health monitoring and frailty prevention in elderly care. Hence, we resorted to another public dataset [4], available in the UCI Machine Learning Repository [18]. The subjects have worn the smartphone on the waist and simulated six different activities. This dataset was built using an accelerometer and a gyroscope. Hence, the considered sensing unit in this subsection was IMU since a magnetometer was not included. As seen in the previous subsection, IMUs are sufficient for this application
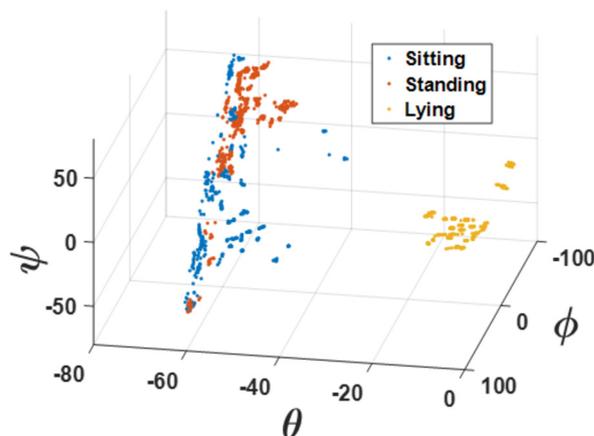

Fig. 6. The distribution of body postures following the mean values of Euler angles.

Table 2

The achieved accuracy of each ML classifier when it comes to the detection of body posture.

	Machine Learning Classifier					
	NN	SVM$_R$	RF	Ada	NB	LDA
Madgwick	**89.6**	**87.8**	87	**88.2**	**88.7**	87.2
Mahony	88	87.2	**87.4**	84.7	87.9	**87.8**

Fig. 7. The confusion matrix resulting from tri-class classification using NN. The columns and rows represent the actual classes and the output of the classifier respectively.

since the estimation of the body posture is done while the subject is being sedentary. As mentioned previously, this task is a tri-class classification, where the targeted classes were (i) Sitting (C_1), (ii) Standing (C_2), and (iii) Lying (C_3). Euler angles were estimated from 2.56-second windows (provided by the authors of this dataset). Three features were calculated, namely the mean values of ϕ, θ, and ψ. Fig. 6 illustrates the distribution of these posture classes following the three extracted features.

Madgwick's filter vs Mahony's filter - The choice of the sensing unit being fixed, both filters are now investigated for this task. Firstly, and based on a simple observation, it is clear that the third class (lying) was well separated from the other two classes. However, a significant intersection exists between Sitting and Standing clusters. Now, to predict the posture of the human body, the mean values (feature vectors of length three) fed a set of machine learning (ML) classifiers. These classifiers were the following ones: (a) Neural Network (NN) with 2 hidden layers of 8 and 2 neurons respectively, and 'ReLU' as activation function; (b) Support Vector Machine with a radial basis function kernel (SVM$_R$); (c) Random Forest (RF) with 20 estimators of depth equal to 2; (d) Adaboost (Ada) with 100 estimators; (e) Naive Bayes (NB) with a Gaussian Distribution; (f) Linear Discriminant Analysis (LDA). Table 2 illustrates the different results. Both orientation filters provided close results in terms of performance, except for NN and Ada. NN achieved the highest accuracy (equal to 89.6%)and Fig. 7 illustrates the corresponding confusion matrix. The confusion occurred between Sitting and Standing, where 20.77% of windows representing
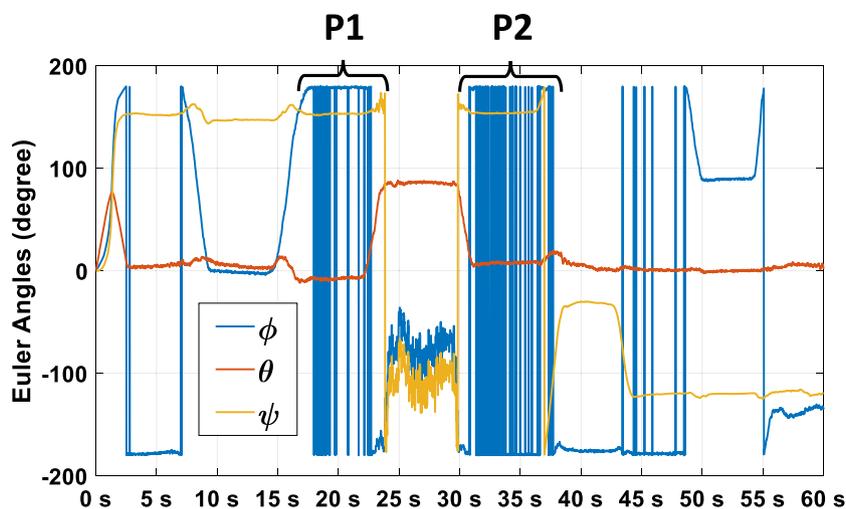
Fig. 8. The estimation of Euler angles using a MARG sensor which was placed close to an electronic device during phases P1 and P2.

Sitting (C_1) were misclassified as Standing (C_2) whereas 11.27% of C_2 were misclassified as C_1. The waist position alone does not seem to be sufficient for this task. Another position and/or additional features are required to increase the achieved accuracy. As seen in Table 2, Madgwick's algorithm had the upper edge when it comes to predicting the body posture with $F_s = 50$ Hz. These results are coherent with the previous sections, where it was seen that Mahony's filter requires a relatively higher sampling rate.

4. Drawbacks and practical considerations

In this section, we discuss some artifacts and limitations related to an attitude estimation system. We have seen in section 3 that MARG sensors are preferred to IMUs when it comes to postural transitions estimation. Now, electronic devices, ferrous materials, and some other mechanical and electrical infrastructures are sources of magnetic fields. These artificial fields contaminate the Earth's magnetic field measurements and decrease the reliability of sensor fusion techniques in heavily disturbed areas like indoor environments [3]. Hence, the indoor performance of MARG sensors could be limited. Fig. 8 illustrates this phenomenon. The Euler angles are estimated using a MARG sensing unit, which was approached close to an electronic device during phases P1 and P2. It is clear that time-series are noisy during both phases, verifying the aforementioned drawbacks.

The use of a gyroscope is required for the attitude estimation, whether the system is based on an IMU or a MARG sensor. However, its power consumption is very high compared to that of the accelerometer [12], which reduces the battery life and the autonomy of the sensing device. This could affect the acceptability of the system, especially when the targeted population is elderly, seeing that the device needs to be recharged frequently.

High sampling rates increase the computational load of attitude estimation systems. The general tendency is to lower it in order to reduce the complexity. However, very low rates may not be able to capture certain movements, thus not sufficient for certain applications. Therefore, the trade-off between accuracy and complexity should be considered when developing such approaches. It is worth mentioning that a sampling rate of 50 Hz leads to satisfactory performance [14].

5. Conclusion

This paper discussed the attitude estimation of inertial sensors. Based on widely used orientation filters, a GUI tool has been developed to visualize the orientation of a rigid body (a sensing device) in a three-dimensional space. The previous study was enriched by discussing two new modules, *i.e.* the option to choose between (1) IMU and MARG as the input device and (2) Madgwick's algorithm and Mahony's algorithm as an orientation filter. This paper addressed the different aspects of attitude estimation systems. It was shown that Madgwick's algorithm is better suited for low sampling rate F_s, whereas Mahony's filter achieves better result for higher rates. Moreover, MARG sensors are preferred to IMUs when it comes to the detection of postural transitions, since the latter might induce high variability when the subject is moving and could produce fast transitions in time-series representing Euler angles which affects the processing units and leads to biased results.

In a future work, modeling the part of the human body where the device is worn in the 3D space should be targeted instead of a simple parallelepiped representing the device, since the orientation of the human body itself is more meaningful for the medical staff. The acceptability of the proposed system will also be investigated.

Human and animal rights

The authors declare that the work described has not involved experimentation on humans or animals.

Funding

Author contributions

All authors attest that they meet the current International Committee of Medical Journal Editors (ICMJE) criteria for Authorship.

CRediT authorship contribution statement

Manuel Abbas: conceptualization, methodology, data acquisition and interpretation, original draft. **Majd Saleh:** conceptualization, methodology, validation, data acquisition. **Joaquim Prud'homm:** investigation, review & editing. **Fabien Lemoine:** investigation, review & editing. **Dominique Somme:** review & editing, project administration, funding acquisition, supervision.

Régine Le Bouquin Jeannès: data acquisition, review & editing, project administration, funding acquisition, supervision.

Declaration of competing interest

The authors declare that they have no known competing financial or personal relationships that could be viewed as influencing the work reported in this paper.

Appendix A

The video can be found on Google drive: https://drive.google.com/file/d/1KqL0oahTCC4jkoFwQAX7E5LWkXDNVqIJ/view. Its goal is to display the simulated fall with both MARG estimation (on the left) and IMU estimation (on the right), using Madgwick's algorithm. Note that the user can select the sensing unit as well as the orientation filter before launching the 3D visualization.

References

[1] Abbas M, Le Bouquin Jeannès R. Exploiting local temporal characteristics via multinomial decomposition algorithm for real-time activity recognition. IEEE Trans Instrum Meas 2021;70:1–11.

[2] Abbas M, Somme D, Le Bouquin Jeannès R. D-sorm: a digital solution for remote monitoring based on the attitude of wearable devices. Comput Methods Programs Biomed 2021;208:106247.

[3] Afzal M, Renaudin V, Lachapelle G. Assessment of indoor magnetic field anomalies using multiple magnetometers. In: 23rd international technical meeting of the satellite division of the institute of navigation (ION GNSS 2010); 2010. p. 525–33.

[4] Anguita D, Ghio A, Oneto L, Parra X, Reyes-Ortiz JL. A public domain dataset for human activity recognition using smartphones. In: 21st European symposium on artificial neural networks (ESANN); 2013.

[5] Bachmann ER, McGhee RB, Yun X, Zyda MJ. Inertial and magnetic posture tracking for inserting humans into networked virtual environments. In: Proceedings of the ACM symposium on virtual reality software and technology. New York, NY, USA: Association for Computing Machinery; 2001. p. 9–16.

[6] Barshan B, Durrant-Whyte H. Inertial navigation systems for mobile robots. IEEE Trans Robot Autom 1995;11:328–42.

[7] Ferrer-Lluis I, Castillo-Escario Y, Montserrat JM, Jané R. Analysis of smartphone triaxial accelerometry for monitoring sleep-disordered breathing and sleep position at home. IEEE Access 2020;8.

[8] Haghi M, Thurow K, Stoll R. Wearable devices in medical Internet of things: scientific research and commercially available devices. Healthc Inform Res 2017;23:4–15.

[9] Han H, Jang H, Yoon SW. Novel wearable monitoring system of forward head posture assisted by magnet-magnetometer pair and machine learning. IEEE Sens J 2020;20:3838–48.

[10] Hwang DY, Chet Ng P, Yu Y, Wang Y, Spachos P, Hatzinakos D, et al. Hierarchical deep learning model with inertial and physiological sensors fusion for wearable-based human activity recognition. In: IEEE international conference on acoustics, speech and signal processing (ICASSP); 2022. p. 21–5.

[11] Kok M, Schön T. A fast and robust algorithm for orientation estimation using inertial sensors. IEEE Signal Process Lett 2019;26:1673–7.

[12] Liu Q, Williamson J, Li K, Mohrman W, Lv Q, Dick RP, et al. Gazelle: energy-efficient wearable analysis for running. IEEE Trans Mob Comput 2017;16:2531–44.

[13] Lu L, Zhang J, Xie Y, Gao F, Xu S, Wu X, et al. Wearable health devices in health care: narrative systematic review. JMIR mHealth uHealth 2020;8:e18907.

[14] Madgwick S. An efficient orientation filter for inertial and inertial/magnetic sensor arrays. https://courses.cs.washington.edu/courses/cse466/14au/labs/l4/madgwick_internal_report.pdf, 2010.

[15] Madgwick SOH, Harrison AJL, Vaidyanathan R. Estimation of imu and marg orientation using a gradient descent algorithm. In: 2011 IEEE international conference on rehabilitation robotics; 2011. p. 1–7.

[16] Mahony R, Hamel T, Pflimlin JM. Nonlinear complementary filters on the special orthogonal group. IEEE Trans Autom Control 2008;53:1203–18.

[17] Michel T, Genevès P, Fourati H, Layaïda N. On attitude estimation with smartphones. In: 2017 IEEE international conference on pervasive computing and communications (PerCom); 2017. p. 267–75.

[18] Reyes-Ortiz J, Anguita D, Ghio A, Oneto L, Parra X. Human activity recognition using smartphones data set. https://archive.ics.uci.edu/ml/datasets/Human+Activity+Recognition+Using+Smartphones, 2012.

[19] Saleh M, Abbas M, Le Bouquin Jeannès R. Fallalld: an open dataset of human falls and activities of daily living for classical and deep learning applications. IEEE Sens J 2021;21:1849–58.

[20] Sevil M, Rashid M, Askari MR, Maloney Z, Hajizadeh I, Cinar A. Detection and characterization of physical activity and psychological stress from wristband data. Signals 2020;1:188–208.

[21] To G, Mahfouz M. Quaternionic attitude estimation for robotic and human motion tracking using sequential Monte Carlo methods with von Mises-Fisher and nonuniform densities simulations. IEEE Trans Biomed Eng 2013;60:3046–59.